ANALYTICA CHIMICA ACTA 614 (2008) 46–57

available at www.sciencedirect.com

ScienceDirect

journal homepage: www.elsevier.com/locate/aca

Second-order advantage from kinetic-spectroscopic data matrices in the presence of extreme spectral overlapping A multivariate curve resolution—Alternating least-squares approach

María J. Culzoni[a], *Héctor C. Goicoechea*[a,*], *Gabriela A. Ibañez*[b], *Valeria A. Lozano*[b], *Nilda R. Marsili*[a], *Alejandro C. Olivieri*[b,**], *Ariana P. Pagani*[b]

[a] *Laboratorio de Desarrollo Analítico y Quimiometría (LADAQ), Cátedra de Química Analítica I, Facultad de Bioquímica y Ciencias Biológicas, Universidad Nacional del Litoral, Ciudad Universitaria, Santa Fe S3000ZAA, Argentina*

[b] *Departamento de Química Analítica, Facultad de Ciencias Bioquímicas y Farmacéuticas, Universidad Nacional de Rosario and Instituto de Química Rosario (IQUIR-CONICET), Suipacha 531, Rosario S2002LRK, Argentina*

ARTICLE INFO

Article history:
Received 16 December 2007
Received in revised form
5 March 2008
Accepted 6 March 2008
Published on line 14 March 2008

Keywords:
Multivariate curve resolution
Kinetic-spectral data
Second-order advantage
Extreme spectral overlapping

ABSTRACT

Multivariate curve resolution coupled to alternating least-squares (MCR-ALS) has been employed to model kinetic-spectroscopic second-order data, with focus on the achievement of the important second-order advantage, under conditions of extreme spectral overlapping among sample components. A series of simulated examples shows that MCR-ALS can conveniently handle the studied analytical problem unlike other second-order multivariate calibration algorithms, provided matrix augmentation is implemented in the spectral mode instead of in the usual kinetic mode. The approach has also been applied to three experimental examples, which involve the determination of: (1) the antiparkinsonian carbidopa (analyte) in the presence of levodopa as a potential interferent, both reacting with cerium (IV) to produce the fluorescent species cerium (III) with different kinetics; (2) Fe(II) (analyte) in the presence of the interferent Zn(II), both catalyzing the oxidation of methyl orange with potassium bromate; and (3) tartrazine (analyte) in the presence of the interferent brilliant blue, both oxidized with potassium bromate, with the interferent leading to a product with an absorption spectrum very similar to tartrazine. The results indicate good analytical performance towards the analytes, despite the intense spectral overlapping and the presence of unexpected constituents in the test samples.

1. Introduction

Kinetic-spectroscopic systems provide analysts with valuable information which can be employed for analytical purposes [1,2]. Kinetic data have been traditionally employed for the determination of single or multiple analytes, based on differential or integrated kinetic equations, with a number of methodologies which vary from application to application [1–3]. For example, the method of proportional equations has been applied to binary mixtures under first- or pseudo first-

* *Corresponding author*. Tel: +54 342 4575205; fax: +54 342 4575205.
** *Corresponding author*. Tel.: +54 341 4372704; fax: +54 341 4372704.
E-mail addresses: hgoico@fbcb.unl.edu.ar (H.C. Goicoechea), aolivier@fbioyf.unr.edu.ar (A.C. Olivieri).
0003-2670/$ – see front matter © 2008 Elsevier B.V. All rights reserved.
doi:10.1016/j.aca.2008.03.013

order conditions [1]. However, only a small fraction of the kinetic data was used, leading to poor precision. Procedures based on Kalman filtering [4,5] and nonlinear least-squares fitting [6] have also been proposed. Multi-component analysis has been attempted by applying principal component regression (PCR), partial least-squares (PLS) or net analyte signal methods, all of which may correct for the effects of component interactions [7-17].

The time evolution of spectra for a reacting system constitutes second-order instrumental data which can in principle be subjected to the successful second-order multivariate calibration methodology [18]. The latter is expected to provide improved analytical results, because single-wavelength kinetic data may be less informative than the multi-wavelength counterpart [19–23]. More importantly, second-order data may show the intrinsic property of the second-order advantage [24], which in principle permits analyte quantitation in samples containing unexpected components, i.e., compounds not included in the calibration set. This property has immense potentialities in the field of complex sample analysis, and allows one to train a calibration model with a limited number of standards, yet quantitating the analyte in the presence of any number of interferents. Some literature examples where kinetic-spectroscopic information has been employed to achieve the second-order advantage can be cited: the determination of creatinine in the presence of serum constituents (albumin, billirubin and glucose) [25], the pesticides carbaryl and chlorpyrifos in commercial samples containing an unexpected substance [26], nitrite in water and meat samples [27], and amoxicillin in urine samples [28].

Second-order algorithms obtaining the second-order advantage are parallel factor analysis (PARAFAC) [29], the generalized rank annihilation method (GRAM) [30], direct trilinear decomposition (DTLD) [31], multivariate curve resolution-alternating least-squares (MCR-ALS) [32], bilinear least-squares (BLLS) [33,34], and alternating trilinear decomposition (ATLD) [35] and its variants self-weighted alternating trilinear decomposition (SWATLD) [36] and alternating penalty trilinear decomposition APTLD [37,38]. Second-order data can also be unfolded into vectors and then subjected to a first-order algorithm, leading to unfolded-PCR (U-PCR) and unfolded-PLS (U-PLS) [39]. A promising alternative is to apply multidimensional PLS (N-PLS) [20], which is a genuine multiway method. However, all of these latter methods do not obtain the second-order advantage, unless they are coupled to a separate procedure known as residual bilinearization (RBL) [40]. Thus U-PLS/RBL, for example, is a promising method enjoying all the capabilities of latent factors methodologies, yet preserving the important second-order advantage [41]. It is interesting to note that the combination of N-PLS/RBL has been suggested in this regard [16,17], although the pertinent algorithm is still under development and testing [42].

An important aspect related to the analysis of second-order kinetic-spectral data is the fact that analytes, and also potential interferents, may show different reaction rates but identical spectra (either themselves or through reagents and products). For example, if sample components react with a reagent to yield either a common UV-visible absorbing or a luminescent reaction product, then the second-order data will show identical profiles in the spectral dimension. The same situation will be encountered when a responsive reagent is consumed by reaction with the sample components. The structure of most second-order algorithms is such that they cannot deal with extreme overlapping in the spectral dimension *between the analyte and the potential interferents*. This phenomenon can be considered as a specific case of linear dependency among component profiles. One way to cope with this problem is to include the potential interferents in the calibration set of samples. This has the disadvantage of requiring knowledge of all possible interferents which can be found in new samples, and leads to a considerable increase in the size of the calibration set.

MCR-ALS is an algorithm which can solve the problems brought about by the presence of linear dependency by resorting to the mathematical resource of matrix augmentation. The latter procedure consists of constructing an augmented data matrix by assembling instrumental data matrices for different samples in the following modes: (1) in the direction of the columns; (2) in the direction of the rows; or (3) in both directions simultaneously. In kinetic-spectroscopic systems, it is usual to augment the matrices in the direction of the reaction time, because this alleviates the problems associated with sample to sample differences in reaction rates. In the presently discussed case, it is preferable to augment in the spectral direction, because this permits differentiation between the analyte and the interferents, as will be shown below. It should be noticed that PARAFAC2, a variant of PARAFAC, is also able to cope with linear dependencies, and may also be employed for the presently discussed analysis [43].

In this report, we present a simulation study of kinetic-spectroscopic systems, which confirms that in the presence of extreme overlapping between the spectra of the analyte and the interferent, the second-order advantage can only be achieved using MCR-ALS as processing algorithm, selecting the spectral direction for matrix augmentation. Furthermore, when the spectra are not identical but highly overlapped, it may be convenient to retain the spectral augmentation mode, depending on the degree of spectral overlap. We also present three experimental kinetic-spectroscopic systems: (1) the reaction of the antiparkinsonian drug carbidopa (the analyte) with cerium (IV) to produce the fluorescent species cerium (III), in the presence of levodopa as potential interferent, which does also react with cerium (IV), but with a different kinetics [44]; (2) the oxidation of methyl orange with potassium bromate, catalyzed by Fe(II) (the analyte), in the presence of Zn(II) as an interferent, which does also catalyze the reaction, but with a different kinetics [45]; and (3) the reaction of tartrazine (the analyte) with potassium bromate [catalyzed by Fe(II)] in the presence of brilliant blue as interferent, which reacts producing a compound with an absorption spectrum very similar to tartrazine. These experimental systems do also show the importance of correctly selecting MCR-ALS as the processing algorithm, using the right augmentation mode depending on the degree of spectral overlap.

In the present work we show that application of MCR-ALS in the spectral augmentation mode is a requirement when identical component profiles occur in the spectral dimension. In the case of poor (but non-zero) spectral selectivity, it is worth to check both augmentation modes, in order to assess

which mode provides the better analytical figures of merit. We provide the first simulated and experimental realization of the processing of this type of intensely overlapped spectral systems, with the aim of accurately quantitating analytes in complex interfering systems.

2. Experimental

2.1. Instrumentation and software

Fluorescence emission spectra for the experimental system 1 were recorded on a Varian Cary Eclypse (Varian, Mulgrave, Australia) luminescence spectrometer equipped with a 7 W Xenon pulse lamp, connected to a PC microcomputer, and using 1.00 cm quartz cells. Instrumental parameters were: excitation and emission slits, 5 nm, λ_{exc} = 255 nm, λ_{em} = 300–400 nm each 5 nm, photomultiplier tube (PMT) sensitivity, 550 mV, scan rate, 3000 nm min^{-1}, averaging time, 0.10 s. The kinetic evolution was followed using 20 scans, recorded every 0.1 min. In this way, the emission-time data matrices had 21 × 20 data points. All measurements were performed in a thermostated cells of 20.0 ± 0.1 °C by means of a RM 6 Lauda thermostatic bath (Lauda, Lauda-Königshofen, Germany).

Electronic absorption measurements for system 2 were carried out on a Perkin Elmer Lambda 20 spectrophotometer (Perkin Elmer, Waltham, Massachusetts, USA), using 1.00 cm quartz cells and 2 nm of slit width. For each sample, twenty spectra were sequentially recorded every 10 s in the wavelength range 450–550 nm every 2 nm, with a scan rate of 2880 nm min^{-1}. Therefore, the size of each spectral-time data matrix was 51 × 20.

System 3 was implemented through a stopped-flow-injection (FIA) system, developed using five modules (degasser, pump, injection valve, autosampler and detector) of an Agilent 1100 Series instrument (Agilent Technologies, Waldbronn, Germany). The flow-injection manifold was designed to inject a sample, previously merged with the reagent, into a Milli-Q water carrier flowing at 0.6 mL min^{-1} through a 200 cm × 0.12 mm i.d. mixing coil. After 12 s since sample injection, the pump was stopped and the reaction was monitored during 108 s. Once this time was reached, the flow was restored. For each FI peak, spectra were registered in the range 400–700 nm each 1 nm, at regular steps 0.4 s for a total time of 120 s. Therefore, matrices of size 301 × 300 per sample were generated, although selected regions (in both dimensions) were subsequently employed for multivariate calibration (see below).

In all cases, spectra were measured in random order with respect to analyte concentrations, and those corresponding to the calibration set were recorded in different days with respect to the validation set. Data were saved in ASCII format, and transferred to a PC Sempron AMD microcomputer for subsequent manipulation by the MCR-ALS program.

2.2. Reagents

All chemicals used were of analytical reagent grade. For the experimental system 1, the following solutions were employed: a 0.25 M H_2SO_4 solution, prepared from concentrated H_2SO_4 (Merck, Darmstadt, Germany). Stock solutions of levodopa 650 mg L^{-1} (Klonal Laboratories, Buenos Aires, Argentina) and carbidopa 500 mg L^{-1} (Klonal Laboratories, Buenos Aires, Argentina) were prepared by weighing the required amount of the corresponding compounds, and dissolved in doubly distilled water after adding eight drops of H_2SO_4 0.25 mol L^{-1}. Both solutions were prepared daily. A stock solution of cerium (IV) (1.00×10^{-3} mol L^{-1}) was prepared from cerium (IV) sulphate tetrahydrate (Merck, Darmstadt, Germany) and dissolved in H_2SO_4 0.25 mol L^{-1}.

For the experimental systems 2 and 3, a stock solution of Fe(II) 1000 mg L^{-1} was prepared by dissolving the appropriate amount of $Fe(NH_4)(SO_4)_2{\cdot}6H_2O$ (Cicarelli, San Lorenzo, Argentina) in water, adding 5.0 mL of H_2SO_4 and diluting to the mark in a 500.00 mL volumetric flask. Solutions of potassium bromate (Cicarelli, San Lorenzo, Argentina) 0.1 mol L^{-1} and phosphoric acid (Cicarelli, San Lorenzo, Argentina) 3.0 mol L^{-1} were also prepared. For system 2, stocks solution of Zn(II) 92.7 mg L^{-1} and methyl orange 1240 mg L^{-1} were prepared from $ZnSO_4{\cdot}7H_2O$ (Merck, Darmstadt, Germany) and from methyl orange (Carlo Erba Reagenti, Milan, Italy), respectively, by dissolving appropriate amounts of each compound in water. For system 3, stock solutions of tartrazine and brilliant blue (Ardinet, Buenos Aires, Argentina) 1000 mg L^{-1} each were also prepared by dissolving appropriate amounts of each compound in water.

Table 1 – Validation concentrations and analyte predictions in the experimental system 1

Validation sample[a]	Levodopa (mg L^{-1})	Carbidopa (mg L^{-1})	
		Nominal	Predicted[b]
1	0.13	0.47	0.47
2	0.46	0.38	0.37
3	0.66	0.28	0.28
4	0.79	0.18	0.16
5	1.06	0.08	0.04
RMSE (mg L^{-1})			0.02
REP%			8.0

[a] RMSE = root mean square error; REP% = relative error of prediction (with respect to the mean calibration concentration).
[b] Average of duplicate analysis.

2.3. Calibration and validation sets

2.3.1. Experimental system 1

For training the multivariate MCR-ALS model, a calibration set was constructed having seven calibration samples for the analyte carbidopa, with concentrations equally distributed in the range 0.00–0.50 mg L^{-1} (six samples) and an additional one at the centre of the latter range, i.e., 0.25 mg L^{-1}.

A five-sample validation set was prepared with the concentrations of carbidopa and levodopa which are reported in Table 1. They were taken at random from the calibration range (carbidopa) and from the range 0.00–1.20 mg L^{-1} (levodopa). These validation solutions were prepared in duplicate, by mix-

Table 2 – Validation concentrations and analyte predictions in the experimental system 2

Validation sample[a]	Iron (II) ($mg\,L^{-1}$)	
	Nominal	Predicted[b]
1	1.00	1.16
2	3.50	3.49
3	5.00	4.92
4	6.50	6.31
5	8.00	7.73
6	9.50	9.45
RMSE ($mg\,L^{-1}$)		0.16
REP%		2.8

[a] RMSE = root mean square error; REP% = relative error of prediction (with respect to the mean calibration concentration). All validation samples contain zinc 3.00 $mg\,L^{-1}$.
[b] Average of duplicate analysis.

ing appropriate volumes of the stock solutions of levodopa and carbidopa.

The oxidation reaction of levodopa and carbidopa was carried out directly in the spectrofluorometer cell. In order to obtain the emission-time matrices, calibration and validation samples were processed as follows: 2.50 mL of the corresponding solution was added to the quartz cell and thermostated at 20 °C for 1 min, and then 200 μL of Ce(IV) 1.00×10^{-3} $mol\,L^{-1}$ dissolved in H_2SO_4 0.25 $mol\,L^{-1}$ were added. The cell was then capped and its content was homogenized turning it upside down. After 10 s, the relative fluorescence of the induced Ce(III) as a function of emission wavelength (21 data points) was recorded during 2 min every 0.1 min (20 reaction times). To remove the effect of the initially present Ce(III), the fluorescence intensities of Ce(IV) solutions were measured daily to obtain appropriate blank corrections.

2.3.2. *Experimental system 2*

A training set of 10 calibration samples was prepared with concentrations of Fe(II) spanning the range 1.00–10.00 $mg\,L^{-1}$ every 1.00 $mg\,L^{-1}$. Additionally, six validation samples containing Fe(II) at different concentrations (see Table 2) were prepared for prediction requiring the second-order advantage, because they also contained 3 $mg\,L^{-1}$ of Zn (II). These validation samples were prepared in duplicate.

The kinetic procedure employed was adapted from the one proposed by Safavi et al. [45]. Suitable amounts of the stock solution of Fe(II) were added to 5.00 mL volumetric flasks containing 1.00 mL of methyl orange 80 $mg\,L^{-1}$ and 1.00 mL of phosphoric acid 3.0 $mol\,L^{-1}$. The samples were then diluted to the mark with Milli-Q water and homogenized. Subsequently, 2.00 mL of each solution were transferred to a 1.00 cm quartz cell and 10 s after the addition of 40 μL of a solution of potassium bromate 0.1 $mol\,L^{-1}$, 20 spectra were sequentially recorded each 10 s.

2.3.3. *Experimental system 3*

A set of six samples was prepared for calibration, with concentrations of tartrazine from 4.00 to 24.00 $mg\,L^{-1}$ each 4.00 $mg\,L^{-1}$. An additional five-sample set was built for validation, having the concentrations of tartrazine and brilliant blue shown in Table 3. These validation samples were prepared in duplicate, by adding 20 μL of the stock solution of the catalyst Fe(II) to 2.00 mL volumetric flasks containing suitable amounts of tartrazine and 40 μL of phosphoric acid 3.0 $mol\,L^{-1}$. The samples were then diluted up to the mark with Milli-Q water and homogenized. An injector program was developed to automatically merge 95 μL of each sample with 5 μL of bromate 0.1 $mol\,L^{-1}$, and to subsequently inject the mixture into the FIA system.

3. Theory

3.1. MCR-ALS

In this second-order multivariate method, an augmented data matrix is created from the calibration and test data matrices. If the matrices are of size $J \times K$ (J is the number of wavelengths and K the number of reaction times), the columns represent the spectral mode and the rows the kinetic mode. The usual setting is to augment matrices in the temporal direction, in order to cope with possible sample to sample variations in kinetic profiles. In the temporal-augmentation mode, the calibration matrices and the unknown matrix are placed adjacent to each other [32]. The bilinear decomposition of the aug-

Table 3 – Validation concentrations and analyte predictions in the experimental system 3

Validation sample[a]	Tartrazine ($mg\,L^{-1}$)			Brilliant blue ($mg\,L^{-1}$)
	Nominal	Predicted[b]	Predicted[c]	Nominal
1	10.00	10.92	13.07	10.00
2	15.00	15.28	16.42	10.00
3	10.00	10.33	11.99	15.00
4	15.00	14.82	15.03	15.00
5	12.50	13.15	13.80	12.50
RMSE ($mg\,L^{-1}$)		0.54	1.63	
REP%		4.4	13.1	

[a] RMSE = root mean square error; REP% = relative error of prediction (with respect to the mean calibration concentration).
[b] Temporal-augmentation mode. The results are averages of duplicate analyses.
[c] Spectral-augmentation mode. The results are averages of duplicate analyses.

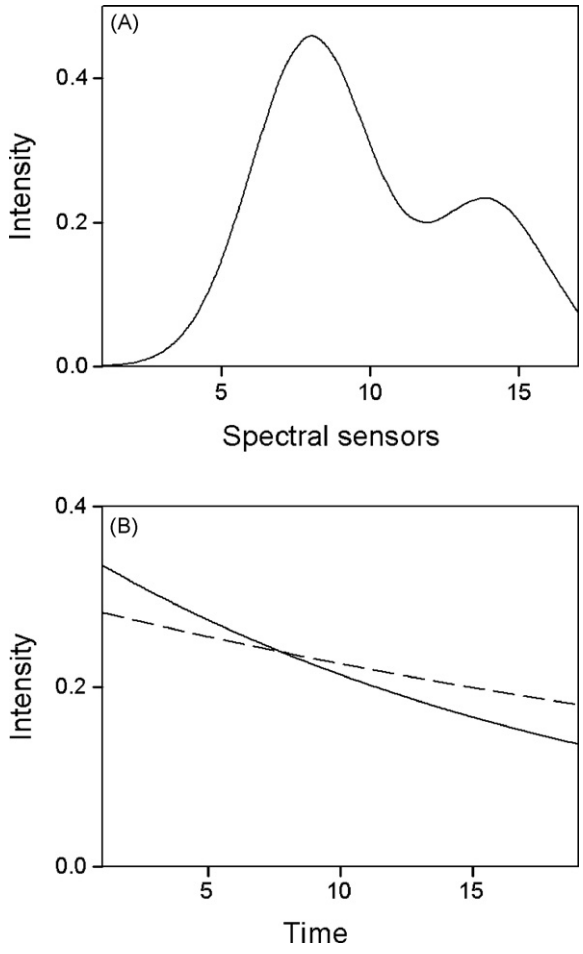

Fig. 1 – (A) Common spectrum to both components of the simulated example 1. (B) Kinetic profiles of both components of the simulated example 1 (solid line, analyte, dashed line, interferent). In all cases, the intensities have been normalized to unit length.

mented matrix is then performed according to the expression:

$$\mathbf{D}_{ta} = \mathbf{S}_{ta}\mathbf{G}_{ta}^{T} + \mathbf{E}_{ta} \quad (1)$$

where the columns of $\mathbf{D}_{ta}$ contain the absorption spectra measured for different samples at several reaction times, the columns of $\mathbf{G}_{ta}$ contain the time profiles of the intervening species, the columns of $\mathbf{S}_{ta}$ their related spectra, and $\mathbf{E}_{ta}$ is a matrix of residuals not fitted by the model (the subscript 'ta' stands for temporal augmentation). Appropriate dimensions of $\mathbf{D}_{ta}$, $\mathbf{G}_{ta}$, $\mathbf{S}_{ta}$ and $\mathbf{E}_{ta}$ are $J \times [(I+1)K]$, $[(I+1)K] \times N$, $J \times N$ and $J \times [(I+1)K]$, respectively (I is the number of training samples, N the number of responsive components and a single test sample is assumed). Decomposition of $\mathbf{D}_{ta}$ is achieved by iterative least-squares minimization of the Frobenius norm of $\mathbf{E}_{ta}$. The minimization is started by supplying estimated spectra for the various components, which are employed to estimate $\hat{\mathbf{G}}_{ta}$ (with the 'hat' implying an estimated matrix) from Eq. (1):

$$\hat{\mathbf{G}}_{ta} = \mathbf{D}_{ta}^{T}(\mathbf{S}_{ta}^{+})^{T} \quad (2)$$

where '+' indicates the generalized inverse. With matrix $\hat{\mathbf{G}}_{ta}$ from Eq. (2) and the original data matrix $\mathbf{D}_{ta}$, the matrix $\mathbf{S}_{ta}$ is re-estimated by least-squares:

$$\hat{\mathbf{S}}_{ta} = \mathbf{D}_{ta}(\hat{\mathbf{G}}_{ta}^{T})^{+} \quad (3)$$

and finally $\mathbf{E}_{ta}$ is calculated from Eq. (1) using $\mathbf{D}_{ta}$ and the estimated $\hat{\mathbf{G}}_{ta}$ and $\hat{\mathbf{S}}_{ta}$ matrices. These steps are repeated until convergence, under suitable constraining conditions during the ALS process, namely non-negativity in spectral and time profiles. The pure spectra of the compounds are expected to be the same in all experiments, while the time profiles in the different $\mathbf{G}_{ta}$ submatrices need not share a common shape. This is the reason why experiments performed in different conditions (e.g. temperature) can be analyzed together as long as the component spectra remain invariant. It is important to point out that MCR-ALS requires initialization with system parameters as close as possible to the final results. One may supply, for example, the species spectra, as obtained from either pure analyte standards or from the analysis of the so-called 'purest' spectra [46]. In the present work we have employed the former alternative in all cases.

The above setting is the regular one when spectra for the intervening species are sufficiently different. In the case of extreme spectral overlapping, however, the generalized inverse required in Eq. (2) becomes unstable. One alternative to solve this problem is to employ the spectral augmentation mode. In this case, the matrices are placed on top of each other, and the least-squares process is represented by the following

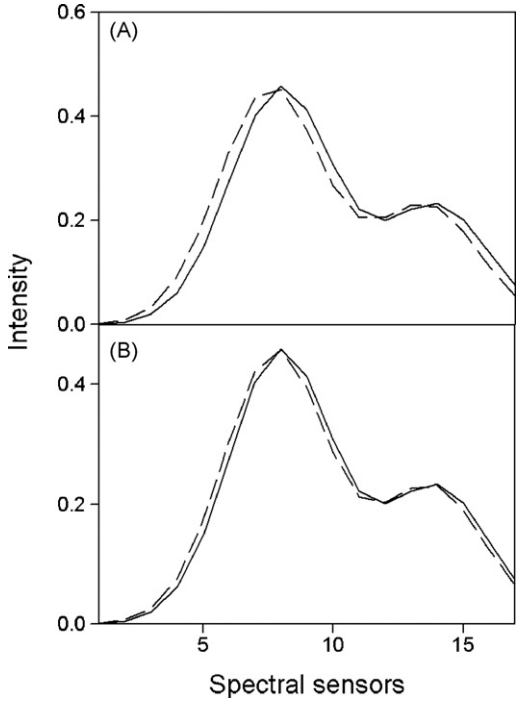

Fig. 2 – (A) Spectra for both components of the simulated example 2. (B) Spectra for both components of the simulated example 3. In both cases, the solid line indicates the analyte and the dashed line the interferent. The intensities have been normalized to unit length.

set of equations:

$$\mathbf{D}_{sa} = \mathbf{S}_{sa}\mathbf{G}_{sa}^{T} + \mathbf{E}_{sa} \quad (4)$$

$$\hat{\mathbf{S}}_{sa} = \mathbf{D}_{sa}(\mathbf{G}_{sa}^{T})^{+} \quad (5)$$

$$\hat{\mathbf{G}}_{sa} = (\hat{\mathbf{S}}_{sa}^{+}\mathbf{D}_{sa})^{T} \quad (6)$$

where now the sizes of the relevant matrices are: $\mathbf{D}_{sa}$, $[(I+1)J] \times K$, $\mathbf{S}_{sa}$, $[(I+1)J] \times N$, $\mathbf{G}_{sa}$, $K \times N$ ('sa' stands for spectral augmentation). In this particular augmentation mode, the generalized inverse of $\mathbf{G}_{sa}$ in Eq. (5) can be obtained provided the kinetic profiles of sample components differ (itself being one of the main assumptions of the present model). More importantly, the generalized inverse of $\mathbf{S}_{sa}$ can also be reliably obtained, because matrix augmentation breaks down the linear dependency of the individual spectral profiles. This is due to the fact that the spectral matrix $\mathbf{S}_{sa}$ has now $[(I+1)J] \times N$ elements instead of the $J \times N$ corresponding to the temporal-augmentation mode. Each column of $\mathbf{S}_{sa}$ consists of successive vectors of size $J \times 1$, each of them having the shape of a particular component spectrum, with an intensity proportional to its concentration in a given sample. Hence, the columns of $\mathbf{S}_{sa}$ are no longer linearly dependent.

After MCR-ALS decomposition of $\mathbf{D}_{sa}$, concentration information contained in $\mathbf{S}_{sa}$ can be used for quantitative predictions, by first building a pseudo-univariate calibration graph with the relative concentrations of the training samples contained in the optimized matrix $\mathbf{S}_{sa}$. Once the particular component of interest is chosen, the elements of $\mathbf{S}_{sa}$ corresponding to the I calibration samples are selected, which run from $S_{sa}(1, n)$ to $S_{sa}(IK, n)$. Each series of K values corresponds to the profile in the time dimension for a particular sample. If the area under the profile is considered as proportional to component concentration, then the required pseudo-univariate graph is built in the following way:

$$\left[\sum_{k=1}^{K} S_{sa}(k, n) \left| \sum_{k=1}^{K} S_{sa}[(k+K), n] \right| \ldots \left| \sum_{k=1}^{K} S_{sa}\{[k+K(I-1)], n\} \right.\right] = k\,\mathbf{y} \quad (7)$$

where each summation groups the K elements of $\mathbf{S}_{sa}$ corresponding to a particular component and standard sample and $\mathbf{y}$ is the vector of calibration concentrations. Once k is found from Eq. (7), subsequent interpolation of the values for the unknown sample provides the concentration of the component in the unknown y_u, i.e.:

$$y_u = \frac{1}{k}\sum_{k=1}^{K} S_{sa}[(k+IK), n] \quad (8)$$

In the regular setting in which augmentation is performed in the temporal mode, Eqs. (7) and (8) are also employed, with $S_{sa}(k, n)$ elements replaced by the analogous series of J elements $G_{ta}(j, n)$ taken from the matrix $\mathbf{G}_{ta}$.

3.2. Simulations

In order to illustrate the behavior of MCR-ALS and other second-order calibration algorithms in connection with the presently studied problem, simulations were carried out for three different systems. In the simulated system 1, a single analyte was considered to be present in the calibration samples, while the latter component and an additional one were included in the test samples. Thus, proper resolution of this system requires adherence to the second-order advantage. The kinetic-spectral matrix data were generated starting

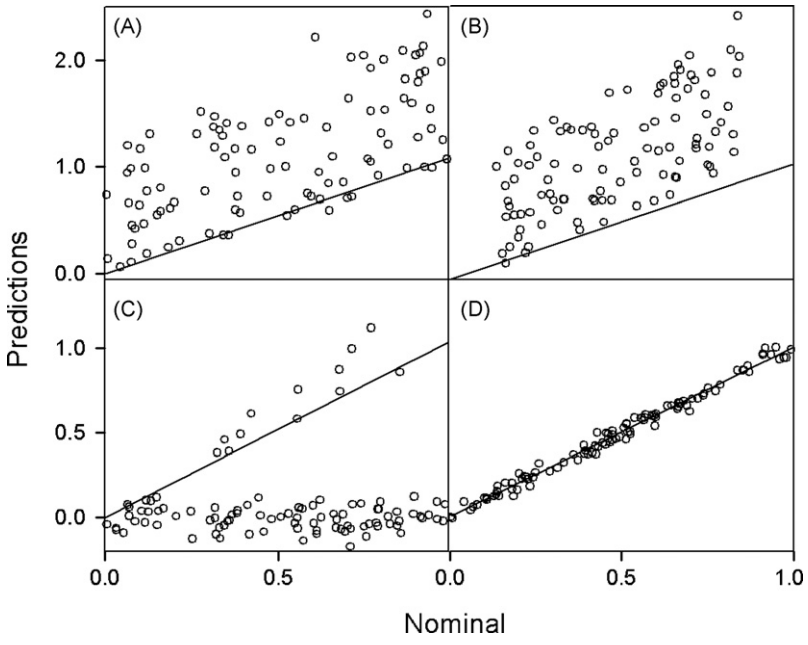

Fig. 3 – Prediction results for the 100 test samples of the simulated example 1 (open circles), using: (A) PARAFAC; (B) GRAM; (C) U-PLS/RBL; (D) MCR-ALS in the spectral augmentation mode. The solid lines indicate the perfect fit.

from noiseless spectral and kinetic profiles which are shown in Fig. 1A and B, respectively. As can be seen, both components have identical spectra, but differ in their reaction rates. From the profiles shown in Fig. 1, a calibration set of second-order signals was built with the analyte at nominal concentrations of 0.3, 0.6 and 0.9 (in arbitrary units). A set of 100 test samples was also created, having random concentrations of both components in the range 0.0–1.0. To all of these second-order signals, noise was added from a gaussian distribution having a standard deviation equal to 5% of the maximum calibration signal.

The second-order data for each of the 100 test samples were then joined to those for the calibration set, and each four-sample data set was submitted to second-order calibration with PARAFAC, GRAM, U-PLS/RBL and MCR-ALS, the latter in the spectral augmentation mode. Specific analyte predictions were stored for statistical analysis and future comparison. In the case of GRAM, the three calibration matrices were averaged to provide a virtual data matrix corresponding to the average analyte concentration in the calibration set. Then the test sample and this virtual sample were subjected to GRAM analysis.

For the simulated systems 2 and 3, the setting was analogous to the simulated system 1, except that slight shifts in the component spectra were allowed (Fig. 2A and B show the corresponding spectra). The time profiles, in turn, were kept at the values shown in Fig. 1B. The results were analyzed using MCR-ALS in both spectral and temporal-augmentation modes, which were compared in order to assess the ability of this algorithm to distinguish components having very similar spectra. A successful spectral distinction would allow one to return to the usual kinetic-augmentation mode, which may provide the additional advantage of coping with changes in kinetic profiles from sample to sample.

In order to quantitate the degree of spectral overlap between components 1 and 2 (S_{12}), the following expression was employed:

$$S_{12} = \frac{||\mathbf{s}_1^T \mathbf{s}_2||}{||\mathbf{s}_1||\,||\mathbf{s}_2||} \quad (9)$$

where $\mathbf{s}_1$ and $\mathbf{s}_2$ are the spectra for components 1 and 2, respectively. The value of S_{12} ranges from zero to one, corresponding to the extreme situations of no overlapping and complete overlapping, respectively. Using Eq. (9), the spectral overlap for the simulated systems 1, 2 and 3 are 1.0000, 0.9936 and 0.9984, respectively, i.e., system 3 shows a degree of overlap which is intermediate between those for systems 1 and 2.

3.3. Software

Simulations were carried out using in-house MATLAB 7.0 routines [47]. When required, the PARAFAC and GRAM algorithms available in the internet were employed [29,48], as well as the routines performing the U-PLS/RBL method [49]. MCR-ALS was implemented using the graphical interface provided by R. Tauler in his web page [50,51].

4. Results and discussion

4.1. Simulations

As explained in Section 3, three simulated systems were analyzed. In the simulated system 1, the spectra of two sample components are identical, while the kinetic profiles differ (Fig. 1). Component 1 is only present in the calibration set, but all test samples contain both constituents.

When PARAFAC was applied to the test samples of this system, the usual methodology in which data for each test sample is joined with those for the calibration samples was employed. Subsequent decomposition of the three-way array, identification of the analyte of interest, and interpolation into the pseudo-univariate calibration graph allows one to predict the concentration of the analyte. The results are shown in Fig. 3A, where the poor recoveries are apparent.

Likewise, use of GRAM by joining each test sample and a virtual sample created by averaging the data matrices for all the calibration samples, led to the results presented in Fig. 3B. Again, the agreement between nominal and predicted concen-

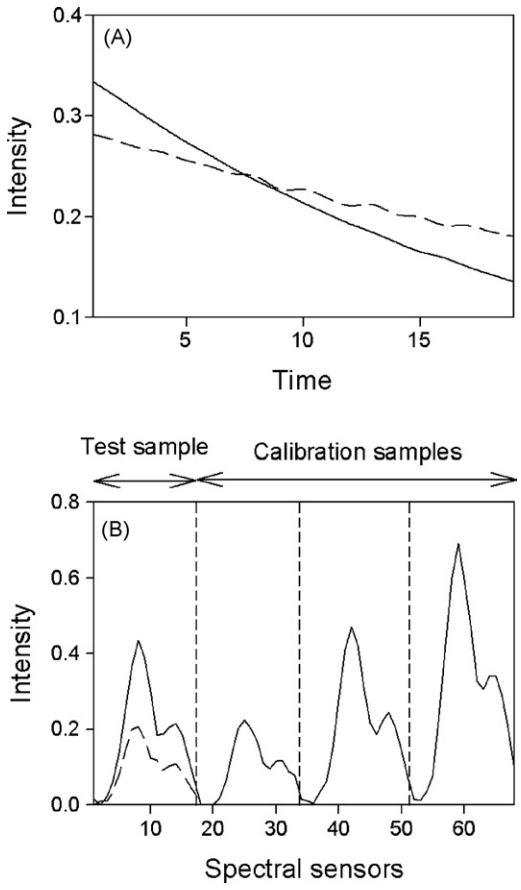

Fig. 4 – Profiles retrieved by MCR-ALS when processing a typical test sample of the simulated example 1. (A) Kinetic profile, common to all samples. (B) Spectral profiles for successive matrix samples in the spectral augmentation mode (test and calibration samples are indicated). In both cases, the solid line indicates the analyte and the dashed line the interferent.

trations is very poor. The U-PLS/RBL method was also applied to this set of samples, calibrating first with the unfolded-PLS algorithm the training data (using a single latent PLS variable), and then implementing the post-calibration RBL procedure in order to obtain the second-order advantage. Poor recoveries are also apparent in Fig. 3C.

MCR-ALS was then employed in the spectral augmentation mode described in the Section 3. Matrix data for each test sample and for the calibration data matrices were placed on top of each other, and decomposition according to Eqs. (4)–(6) was performed by imposing the restriction of non-negativity for both component profiles in both dimensions. Another constraint imposed to the model during ALS minimization was the correspondence among species, i.e., information was supplied on the absence of component 2 in all calibration samples, allowing it to only appear in the test sample. The results (Fig. 3D) shows good agreement between nominal and predicted concentrations values, with an average root mean square error (RMSE) of 0.035 units, implying a relative error of prediction (REP%) with respect to the mean calibration concentration of 5.8%. Fig. 4 shows the profiles retrieved by MCR-ALS in the temporal (Fig. 4A) and spectral (Fig. 4B) dimensions for a typical test sample and the three calibration samples. As can be seen, the kinetics are perfectly distinguished (compare Fig. 4A with Fig. 1B), and the spectra are recognized as belonging to either component 1 (present in all samples) or component 2 (present only in the test sample), as shown in Fig. 4B. It should be noticed that in the above-simulated case, spectral augmentation is the only setting which allows MCR-ALS to solve the analytical problem achieving the second-order advantage.

The simulated systems 2 and 3 provide the opportunity of analyzing the effect of small spectral shifts in the pure component spectra, i.e. spectral overlapping between components which are close to, but not exactly 1. The corresponding spectral profiles are shown in Fig. 2. When MCR-ALS was applied in both temporal- and spectral-augmentation modes for these simulated systems, the obtained results are presented in Fig. 5. Fig. 5A and B show the results for the simulated system 2, using spectral and temporal augmentation, respectively, in a system where the degree of spectral overlap is 0.9936. The corresponding RMSE (REP%) values are 0.026 (4.3%) and 0.020 (3.3%), indicating comparable results for both augmentation modes. The degree of overlap in the time dimension can be calculated with Eq. (9), replacing the spectral profiles with the corresponding time profiles, yielding a value of 0.9916. As can be seen, the overlapping is similar in both dimensions, leading to comparable prediction errors using either augmentation mode.

In the case of the simulated system 3, on the other hand, the RMSE (REP%) are 0.032 (5.3%) and 0.044 (7.3%) for spectral and temporal augmentation, respectively. The corresponding plots of predicted versus nominal can be found in Fig. 5C and D. In this system, where the degree of overlap S_{12} is 0.9984, the worst statistical indicator corresponds to the temporal-augmentation setting. This can be ascribed to spectral superposition leading to instabilities in the computation of the generalized inverse of the pure component spectral $\mathbf{S}_{ta}$ matrix [see Eq. (2)]. In fact, the spectral overlapping is larger than the one in the time dimension (0.9916, see above). Thus, time augmentation yields poorer recoveries in comparison with the augmentation in the spectral direction, which appears to be the method of choice for severe spectral overlapping.

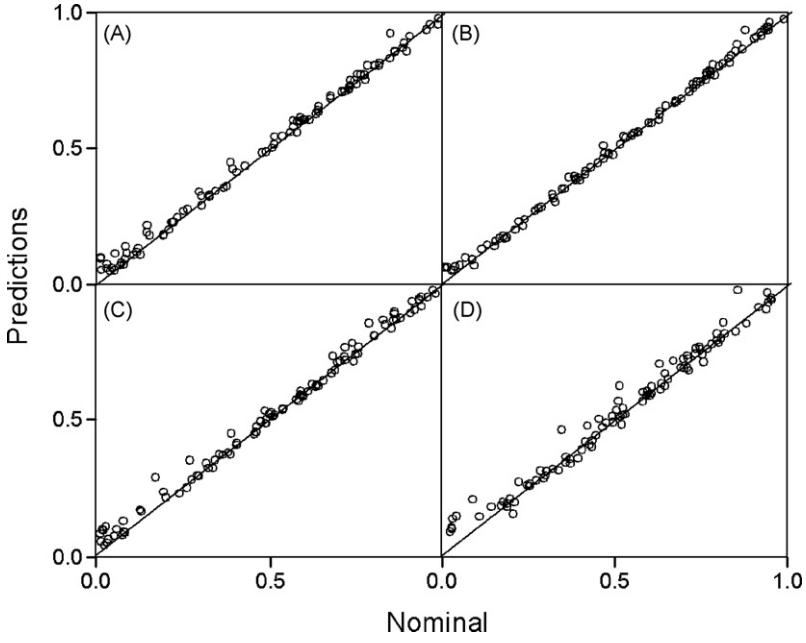

Fig. 5 – Prediction results for the 100 test samples of the simulated examples 2 and 3 using MCR-ALS (open circles): (A) simulated example 2, spectral augmentation mode; (B) simulated example 2, temporal-augmentation mode; (C) simulated example 3, spectral augmentation mode; and (D) simulated example 3, temporal-augmentation mode. The solid lines indicate the perfect fit.

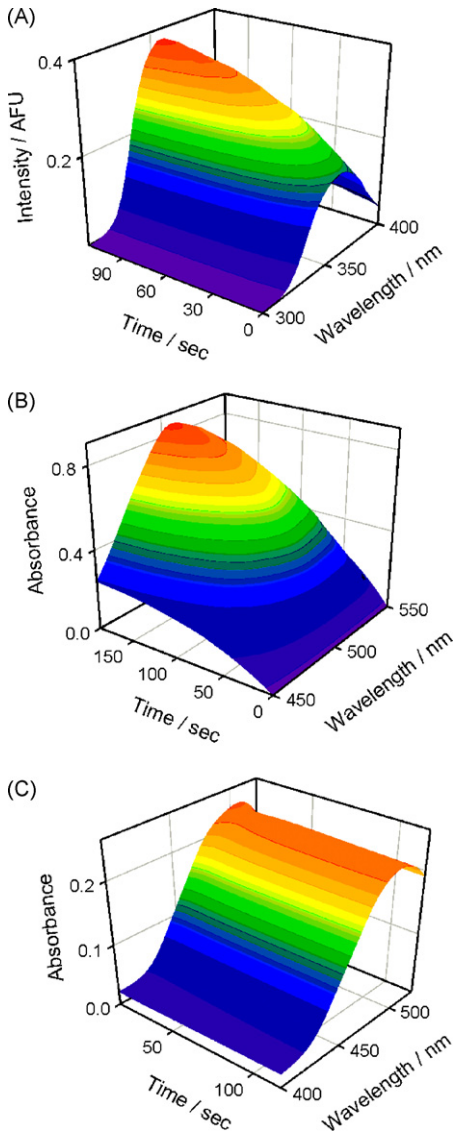

Fig. 6 – Three-dimensional plots of signal as a function of wavelength and reaction time for the studied experimental systems: (A) experimental system 1, fluorescence intensity (AFU = arbitrary fluorescence units) for a calibration sample containing carbidopa 0.40 mg L^{-1}, during reaction with Ce(IV) to produce fluorescent Ce(III); (B) experimental system 2, absorbance for a calibration sample containing 5.00 mg L^{-1}, during reaction with potassium bromate (data were converted as described in the text, i.e., subtracting the spectrum at zero time and taking the modulus); and (C) experimental system 3, absorbance for a validation sample containing 15.0 mg L^{-1} of both tartrazine and brilliant blue during reaction with potassium bromate.

4.2. *Experimental system 1*

Fig. 6A shows the time evolution of the fluorescence intensity in the useful emission range for a typical sample containing carbidopa, during reaction with Ce(IV) to produce the fluorescent Ce(III) species. Similar results are obtained when levodopa is subjected to the same oxidation conditions. It may be noticed that the generation of fluorescent Ce(III) has been previously employed for the analysis of pharmaceuticals, taking advantage of the different oxidation kinetics [17,44]. First-order multivariate calibration methods were employed, which imply the preparation of calibration sets containing all possible responsive components [17,44]. In the present work, the focus is directed towards the achievement of the second-order advantage, and thus the calibration samples only contained carbidopa, while the validation samples contained both components. In view of the identical emission spectra produced by both system components, quantitation of carbidopa in the validation samples is only possible using MCR-ALS in the spectral augmentation mode, in the manner described above for the simulated example 1. It should be noticed that freshly prepared solutions of Ce(IV) produce a blank signal, which was reproducible from sample to sample. Hence, an average blank matrix was subtracted from all sample data matrices, in order to correct for the presence of the blank signal. In this way, only two responsive components were considered during MCR-ALS processing.

Matrix decomposition yielded the kinetic and spectral profiles which are shown in Fig. 7A and B, respectively. As can be seen, the kinetic profiles (Fig. 7A) are sufficiently different to ensure distinguishing both sample components. Moreover, Fig. 7B shows that the presence of the interferent levodopa is correctly accounted for in the test sample, whereas only the calibrated analyte carbidopa is present in the training samples.

The areas under the analyte spectra for each sample in Fig. 7B are proportional to its concentration, a fact which permits analyte quantitation in the test sample, even in the presence of the unexpected interferent. Specifically, this was accomplished using the pseudo-univariate approach represented by Eqs. (7) and (8) for calibration and prediction, respectively. Specific prediction results for the five-sample validation set are presented in Table 1. As can be seen, good statistical indicators are obtained: the RMSE is 0.02 mg L^{-1}, corresponding to an REP of 8.0% based on the mean calibration concentration. This implies that the presently discussed methodology is feasible for attaining the second-order advantage in a case of sample components leading to identical product spectra.

4.3. *Experimental system 2*

In this system, the signal at time zero corresponds to the high absorbance spectrum of methyl orange. The absorbance slowly decreases due to reaction with potassium bromate, catalyzed by the presence of metal ions, in our case Fe(II) (the analyte) and Zn(II) (the potential interferent). In order to enhance the information provided by the experimental data obtained during the reaction, the following data pre-preprocessing was applied: the spectrum at zero time was subtracted from all spectra contained in each data matrix at all times. In this way, differences among kinetic profiles for different samples were highlighted. Subsequently, the moduli of the obtained values were used to build the MCR-ALS models. Fig. 6B shows the time evolution of the matrix data, converted in the manner described above, for a calibration

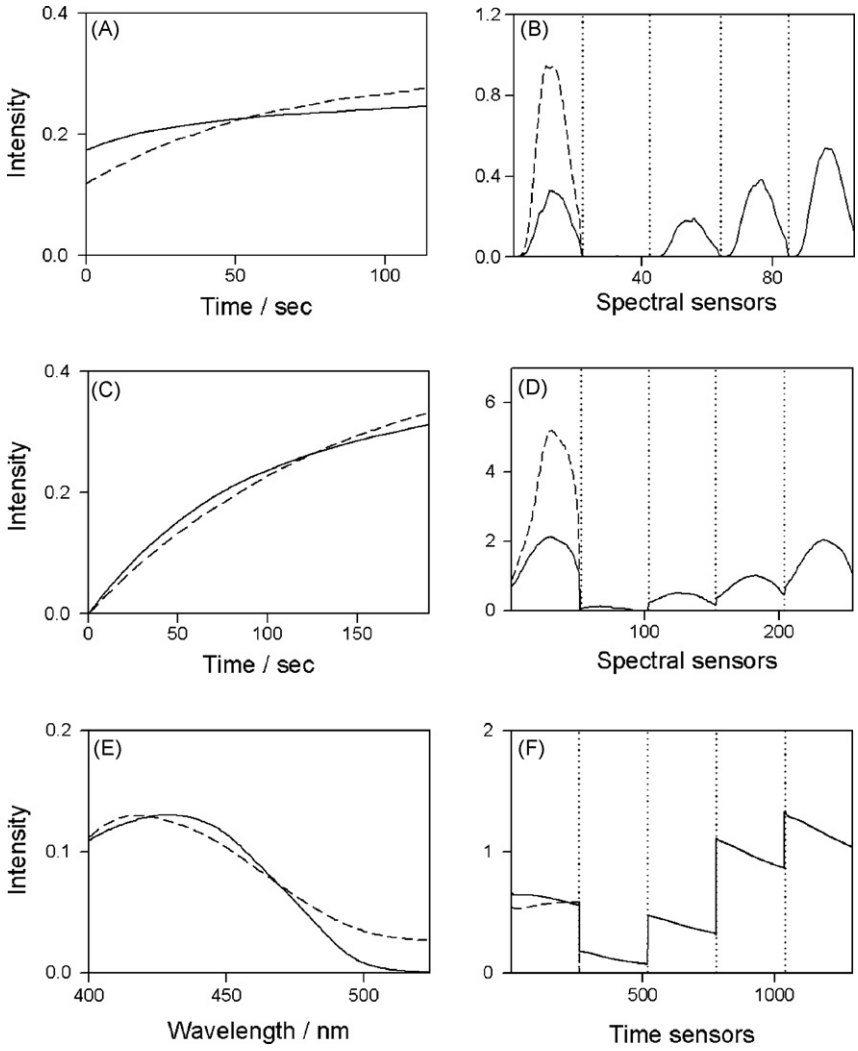

Fig. 7 – Plots of the spectral and kinetic profiles after MCR-ALS processing of a typical test sample, together with the calibration samples, for the experimental systems 1 (A and B), 2 (C and D) and 3 (E and F). Plots (A) and (C) correspond to the kinetic profiles, which are common to all samples in the experimental systems 1 and 2. Plots (B) and (D) show the spectral profiles for successive matrix samples in the spectral augmentation mode (the first sample is the test one and the remaining ones are the first four calibration samples, with vertical dotted lines separating sensor ranges for each sample). Only four calibration samples are shown for simplicity. Plots (E) and (F) correspond to the experimental system 3 when the most successful kinetic augmentation is employed. They are analogous to plots (A)–(D), but the spectral and kinetic modes are interchanged. In all cases, the solid line indicates the analyte and the dashed line the interferent. The profiles in plots (A), (C) and (E) are all normalized to unit length.

sample containing Fe(II) 5.00 mg L^{-1}: absorbance differences which are initially zero at all wavelengths are seen to increase as the reaction progresses.

As previously shown for the simulated system 1 and also for the experimental system 1, this system can only be analyzed using MCR-ALS in the spectral augmentation mode. Thus, the calibration data matrices and each of the validation matrices were placed on top of each other, in order to augment the matrices in the spectral dimension. Decomposition was then performed by imposing the same non-negativity and species correspondence restrictions commented above. The profiles retrieved by the program are shown in Fig. 7C and D in the kinetic and in the (augmented) spectral dimensions, respectively. Notice in Fig. 7C that the profiles show the increase in the absorbance change, since these matrix data were previously converted by subtraction of the spectra at zero time and taking the modulus. Predictive results obtained with pseudo-univariate methodology discussed above are presented in Table 2, showing an excellent agreement between nominal and predicted values: the RMSE is 0.16 mg L^{-1}, implying a REP value of 2.8%.

4.4. *Experimental system 3*

Fig. 6C shows the time evolution of the absorbance in the useful spectral range for a validation sample containing 15.0 mg L^{-1} of both tartrazine and brilliant blue. As mentioned in Section 2, appropriate sensor regions were selected in both

dimensions before building the models. Specifically, wavelengths were restricted to 400–524 nm, and times to 14–115.6 s, leading to 125 × 259 data points per sample, and shown in Fig. 6C for the selected example.

In this experimental system, tartrazine reacts with potassium bromate in the presence of Fe(II), and its absorbance significantly decreases due to the oxidation reaction. The potential interferent brilliant blue, in turn, does also react with bromate, yielding a reaction product whose spectrum is very similar to that of tartrazine, but not identical: the degree of spectral overlap, estimated using Eq. (9), is 0.9856. The only two responsive components in samples having both tartrazine and brilliant blue are therefore the former compound and the oxidation product of the latter. MCR-ALS was applied to this system in both the temporal- and spectral-augmentation modes, with analytical results which are presented in Table 3. As can be seen, better results are furnished when the temporal-augmentation mode is applied, with an RMSE (REP%) of 0.54 (4.4%). On the other hand, a value of RMSE (REP%) of 1.63 (13.1%) is obtained when the spectral-augmentation is implemented. This fact can be ascribed to spectral differences between tartrazine and brilliant blue oxidation product which are large enough to stabilize the generalized inverse of the pure component spectral **S** matrix. In fact, Eq. (9) can be employed to estimate the degree of kinetic overlap between components, by replacing the spectra with the corresponding time profiles. The result is 0.9969, showing a stronger overlap in the time dimension in comparison with the spectral dimension. This is the reason why better analytical figures of merit are obtained in the temporal-augmentation mode.

Fig. 7E and F show the spectral and (augmented) kinetic profiles for a typical test sample and some of the calibration samples after MCR-ALS data processing. The success of the applied chemometric technique in decomposing the contributions of both sample constituents is apparent. Not only the retrieved spectra (Fig. 7E) compare well with the known component spectra, but the kinetic profiles (Fig. 7F) agree with the presence of a growing concentration of the brilliant blue oxidation product in the test sample. In both the test and calibration samples, on the other hand, a time-decreasing concentration of the analyte tartrazine is evident (Fig. 7F).

In this particular experimental system, the differences in spectral profiles provided enough spectral differentiation so that the usual temporal-augmentation mode outperformed the spectral augmentation in what concerns analytical figures of merit. However, in a more severely overlapped system in the spectral dimension, the opposite might be true. Our results indicate that in this case both options should be checked before deciding which provides the better analytical results.

5. Conclusions

Simulations and experimental data for second-order kinetically modulated luminescent and absorptive instrumental data shows that multivariate curve resolution coupled to alternating least-squares is a suitable data processing method. In the presence of extreme spectral overlapping, matrix augmentation in the spectral mode permits an adequate decomposition of the augmented data matrix, leading to the achievement of the second-order advantage. When the extreme overlapping condition is relaxed, differences in component spectra may allow for augmentation in the temporal direction, which is usually employed to cope with sample to sample variations in kinetic profiles. Future analysis of complex samples using kinetic-spectral second-order data may benefit from the presently discussed chemometric approach.

Acknowledgments

Universidad Nacional del Litoral (Project CAI + D N° 12/B604), Universidad Nacional de Rosario, CONICET (Consejo Nacional de Investigaciones Científicas y Técnicas, Project No. PIP 5303) and ANPCyT (Agencia Nacional de Promoción Científica y Tecnológica, Project No. PICT04-25825 and PICTO05-35124) are gratefully acknowledged for financial support. MJC thanks CONICET and VAL thanks ANPCyT for their fellowships.

REFERENCES

[1] H. Mottola, Kinetic Aspects of Analytical Chemistry, John Wiley & Sons, New York, 1988.
[2] D. Perez-Bendito, M. Silva, Kinetic Methods in Analytical Chemistry, Horwood, Chichester, 1988.
[3] X. Wu, R. Cai, L. Zhang, M. Xiao, Anal. Chim. Acta 448 (2001) 257–263.
[4] P.D. Wentzell, M.I. Kazayannis, S.R. Crouch, Anal. Chim. Acta 224 (1989) 263–274.
[5] R. Xiong, A. Velasco, M. Silva, D. Pérez Bendito, Anal. Chim. Acta 251 (1991) 313–319.
[6] A. Cladera, E. Gómez, J.M. Estela, J. Cerdá, V. Cerdá, Anal. Chim. Acta 272 (1993) 339–344.
[7] M. Blanco, J. Coello, H. Iturriaga, S. Maspoch, J. Riba, E. Rovira, Talanta 40 (1993) 261–267.
[8] A. Cladera, E. Gómez, J.M. Estela, V. Cerdá, Anal. Chem. 65 (1993) 707–715.
[9] J. Havel, F. Jiménez, R.D. Bautista, J.J. Arias León, Analyst 118 (1993) 1355–1360.
[10] M. Blanco, J. Coello, H. Iturriaga, S. Maspoch, J. Riba, Anal. Chem. 66 (1994) 2905–2911.
[11] M. Blanco, J. Coello, H. Iturriaga, S. Maspoch, M. Redón, Anal. Chem. 67 (1995) 4477–4483.
[12] J.M. García, A.I. Jiménez, J.J. Arias, K.D. Khalaf, A. Morales-Rubio, M. de la Guardia, Analyst 120 (1995) 313–317.
[13] Y.L. Xie, J.J. Baeza-Baeza, G. Ramis-Ramos, Anal. Chim. Acta 321 (1996) 75–95.
[14] I. Durán-Merás, A. Espinosa Mansilla, F. Salinas López, Analyst 120 (1995) 2567–2571.
[15] Z. Bouhsain, S. Garrigues, M. de la Guardia, Analyst 121 (1996) 1935–1938.
[16] M. de la Guardia, K.D. Khalaf, B.A. Hasan, A. Morales-Rubio, J.J. Arias, J.M. García-Fraga, A.I. Jiménez, F. Jiménez, Analyst 121 (1996) 1321–1326.
[17] A. Muñoz de la Peña, A. Espinosa-Mansilla, M.I. Acedo Valenzuela, H.C. Goicoechea, A.C. Olivieri, Anal. Chim. Acta 463 (2002) 75–88.
[18] G.M. Escandar, N.M. Faber, H.C. Goicoechea, A. Muñoz de la Peña, A.C. Olivieri, R.J. Poppi, Trends Anal. Chem. 26 (2007) 752–765.

[19] J.C.G. Esteves da Silva, C.J.S. Oliveira, Talanta 49 (1999) 889–897.
[20] R. Bro, J. Chemom. 10 (1996) 47–61.
[21] M. Azubel, F.M. Fernández, M.B. Tudino, O.E. Trocoli, Anal. Chim. Acta 398 (1999) 93–102.
[22] A.K. Pettersson, B. Karlberg, Anal. Chim. Acta 354 (1997) 241–248.
[23] J. Coello, S. Maspoch, N. Villegas, Talanta 53 (2000) 627–637.
[24] K.S. Booksh, B.R. Kowalski, Anal. Chem. 66 (1994) 782A–791A.
[25] M.V. Guterres, P.L. Volpe, M.C. Ferreira, Appl. Spectrosc. 58 (2004) 54–60.
[26] A. Espinosa Mansilla, A. Muñoz de la Peña, H.C. Goicoechea, A.C. Olivieri, Appl. Spectrosc. 58 (2004) 83–90.
[27] A. Nazi, J. Ghasemi, A. Yazdanipur, Anal. Lett. 38 (2005) 2377–2392.
[28] A. García-Reiriz, P.C. Damiani, A.C. Olivieri, Talanta 71 (2007) 806–815.
[29] R. Bro, Chemom. Intell. Lab. Syst. 38 (1997) 149–171.
[30] E. Sanchez, B.R. Kowalski, Anal. Chem. 58 (1986) 496–499.
[31] E. Sanchez, B.R. Kowalski, J. Chemom. 1 (1990) 29–45.
[32] A. de Juan, E. Casassas, R. Tauler, in: R.A. Myers (Ed.), Encyclopedia of Analytical Chemistry, vol. 11, Wiley, Chichester, 2002, pp. 9800–9837.
[33] M. Linder, R. Sundberg, Chemom. Intell. Lab. Syst. 42 (1998) 159–178.
[34] M. Linder, R. Sundberg, J. Chemom. 16 (2002) 12–27.
[35] H.L. Wu, M. Shibukawa, K. Oguma, J. Chemom. 12 (1998) 1–26.
[36] Z.P. Chen, H.L. Wu, J.H. Jiang, Y. Li, R.Q. Yu, Chemom. Intell. Lab. Syst. 52 (2000) 75–86.
[37] L.Q. Hu, H.L. Wu, Y.J. Ding, D.M. Fang, A.L. Xia, R.Q. Yu, Chemom. Intell. Lab. Syst. 82 (2006) 145–153.
[38] A.L. Xia, H.L. Wu, D.M. Fang, Y.J. Ding, L.Q. Hu, R.Q. Yu, J. Chemom. 19 (2005) 65–76.
[39] S. Wold, P. Geladi, K. Esbensen, J. Øhman, J. Chemom. 1 (1987) 41–56.
[40] J. Öhman, P. Geladi, S. Wold, J. Chemom. 4 (1990) 79–90.
[41] A.C. Olivieri, J. Chemom. 19 (2005) 253–265.
[42] V.A. Lozano, G.A. Ibañez, A.C. Olivieri, Anal. Chim. Acta 610 (2008) 186–195.
[43] R. Bro, Doctoral Thesis, University of Amsterdam, The Netherlands (1998).
[44] A. Pagani, M.A. Cabezón, G. Ibañez. J. Pharm. Biomed. Anal. (submitted for publication).
[45] A. Safavi, G. Absalan, S. Maesum, Anal. Chim. Acta 432 (2001) 229–233.
[46] W. Windig, J. Guilment, Anal. Chem. 63 (1991) 1425–1432.
[47] MATLAB 7.0, The Mathworks, Natick, Massachusetts, 2003.
[48] http://www.models.kvl.dk/source/.
[49] http://www.chemometry.com.
[50] http://www.ub.es/gesq/mcr/mcr.htm.
[51] J. Jaumot, R. Gargallo, A. de Juan, R. Tauler, Chemom. Intell. Lab. Syst. 76 (2005) 101–110.